

matching at the front face is governed by the *chiro-sorb* condition³ which cannot be met with conventional materials while the absorption is enhanced by the chiral skin depths. More specifically as $k_c \Delta$ becomes large, the equivalent impedance η_L^m approaches η_c and the *chiro-sorb* limit is attained as can be seen in the upper portion of Fig. 1.

The electric *chiroshield*, which is an alternative to the Salisbury screen, is formed by placing a quarter-wavelength spacer between the conductor and the chiral material as shown in the lower half of the left panel of Fig. 1. Following the previous analysis, the field-amplitude reflection coefficient R_e of this geometry is found to be $R_e = (\eta_0 - \eta_L^e)/(\eta_0 + \eta_L^e)$ with

$$\eta_L^e = i\eta_c \cot k_c \Delta \quad (4)$$

representing the equivalent wave impedance at the front interface. For the example given here the spacer impedance is taken to be η_0 . The properties of this shield are not dissimilar to those of the magnetic shield as can be seen from the centre panel of Fig. 1. It can be shown that, for high frequencies and losses, η_L^e will approach η_c as for the magnetic case.

The centre and right panels of Fig. 1 show the reflection coefficient amplitudes for the magnetic (upper) and electric (lower) *chiroshield* and their achiral counterparts, respectively. The vertical axis is a logarithmic measure of the reflection while the frequency axis is a measure of $(\omega - \omega_0)/\omega_0$ where ω is the radian frequency of the incident wave. The chiral material thickness is $\Delta = 0.2\lambda$ where λ is the free-space wavelength corresponding to ω_0 . The loss axis is a measure of the loss tangent μ^i/μ^r for the two cases under consideration where the superscripts i and r indicate imaginary and real parts, respectively. Here the degree of chirality is specified to be $\xi_c = 1/\eta_0$. The desirable low plateau of relatively constant reflection amplitude is characteristic of these two chiral screens and is found over a broad range of frequency and loss values. The reduction in the level of reflection achieved by the *chiroshield* as compared with its conventional counterparts is remarkable, even for thin screens. For example, a chiral magnetic screen of this design with thickness $\lambda/6$ produces an additional reduction in reflection of approximately 20 dB as compared to its achiral counterpart for a loss tangent of approximately 4. Such reduction is enhanced with increasing loss because of the advantageous effect of chirality.

In summary, we have provided a means for the control of radar cross-section of conducting surfaces through chiral coatings we call *chiroshield*. These techniques may also be used for coated composites. Chirality offers additional degrees of freedom which are manifest through the complex chirality admittance ξ_c . With this extra flexibility, chirality is able to increase average absorption throughout the coating and enhance the impedance matching. The advantages offered by *chiroshield* include a ~ 20 dB to ~ 30 dB reduction in reflection over its conventional counterpart and a significant increase in bandwidth for the cases examined here. Applications to additional planar and non-planar geometries will be presented shortly.

The words *chiro-sorb* and *chiroshield* are trade marks, and a patent is pending on the latter.

D. L. JAGGARD
N. ENGHETA
J. LIU

13th June 1990

Complex Media Laboratory
Moore School of Electrical Engineering
University of Pennsylvania
Philadelphia, PA 19104, USA

References

- 1 See e.g., FANTE, R. L., and MCCORMACK, M. T.: 'Reflection properties of the Salisbury screen', *IEEE Trans.*, 1988, **AP-36**, pp. 1443-1454
- 2 JAGGARD, D. L., MICKELSON, A. R., and PAPAS, C. H.: 'On electromagnetic waves in chiral media', *Appl. Phys.*, 1979, **18**, pp. 211-216
- 3 JAGGARD, D. L., and ENGHETA, N.: 'Chiro-sorb as an invisible medium', *Electron. Lett.*, 1989, **25**, pp. 173-174
- 4 BASSIRI, S., PAPAS, C. H., and ENGHETA, N.: 'Electromagnetic wave propagation through a dielectric-chiral interface and through a chiral slab', *J. Opt. Soc. Am. A*, 1988, **5**, pp. 1450-1459

RIGOROUS DISPERSIVE ANALYSIS OF SKIN EFFECTS ON A PRINTED MICROSTRIP LINE CONTAINING FINITE CONDUCTOR LOSSES

Indexing terms: Microstrip, Skin effect

Theoretical full-wave analyses of skin effects on a microstrip line plated with 1 mil (1/1000 inch) thick gold conductor are presented. The time-harmonic complex longitudinal and transverse current distributions inside and on the surface of the metal strip are reported for a microstrip operating at 100 GHz. The case study shows that the current distributions obtained by the new full-wave approach agree well with those predicted by the well-known plane analysis of skin effects.

Introduction: The increasing use of planar and/or quasi-planar transmission lines in millimetre-wave and microwave monolithic integrated circuits (MMICs) has made the dissipative conductor losses of these structures an important issue.¹ The analysis of conductor losses must be coupled with the finite metal thickness in MMIC design.² Recently a few full-wave field-theoretic methods analysing the conductor losses of the transmission lines have been reported.³⁻⁵ This letter extends the full-wave approach of Reference 5 by incorporating the concept of network equivalent representation of the mode-matching method,⁶ thereby easily formulating the non-standard eigenvalue equation associated with transmission line conductor loss problems. The time-harmonic complex longitudinal and transverse current distributions are found rigorously for the case of a microstrip with structural and material parameters shown in Fig. 1, and with a 1 mil (1/1000 inch) thick gold metal coating on the strip. Unless the full-wave formulation is accurate, such complex current distributions are difficult to solve accurately. The well-known skin effect plane analysis of the current distribution,⁷ which is applicable for the case of thick and good conductor coating, validates the results obtained by the new formulation.

Formulation: The full-wave hybrid TE-to-y and TM-to-y fields in regions I, II, and III of Fig. 1 are in terms of eigenfunction expansions, which are classified as either air or metal modes in References 5, satisfying the required boundary conditions in the y direction. Next the network equivalents of the interfaces at $x = 0$ and $x = w$ are employed.⁶ Between the interfaces or between the interface and the perfectly conducting side wall, the equivalent circuits are essentially transmission line analogies. Thus after applying the resonance condition along the x direction, a nonstandard eigenvalue equation can be readily derived. The roots of this equation are the complex propagation constants of the lossy transmission line. The conduction current density J is the product of σ (conductivity of the metal strip) and E (electric field vector). J

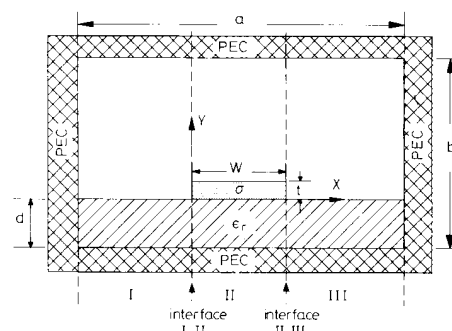


Fig. 1 Shielded microstrip line with thick gold metal coating

Structural and material parameters:
 $f = 100$ GHz, $\epsilon_r = 2.22$, $d = 10$ mils, $w = 0.73$ mm, $t = 1$ mil
 $a = 2b = 2.54$ mm, $\sigma = 3.33 \times 10^7$ mho/m, $t/\delta = 92.1$
 $\delta =$ skin depth of gold at 100 GHz = 0.276 μ m
 PEC = perfect electric conductor

consists of two parts. The longitudinal part is the current flowing along the z direction. The transverse part is the current flowing on the x - y plane. For the transverse currents, only the x components are presented in this letter.

Skin effects on a microstrip with thick and good conductor coating: Given the structural and material parameters shown in Fig. 1, the skin depth is $0.276\ \mu\text{m}$ at 100 GHz. The t/δ (thickness of the strip to skin depth) ratio is 92.1. This is a conceivably thick metal coating. Figs. 2 and 3 are plots of the normalised complex current distributions with the left vertical scale showing magnitude and the right vertical scale showing phase. A set of curves is generated by the new full-wave formulation using the parameters representing the penetration depth of the electromagnetic waves into the metal strip. The surface currents are located at $y = 0$, $y = t$, $x = 0$, and $x = w$. Only parts of the current distributions are shown because of the symmetry of the structure. The left hand sides of Figs. 2 and 3 are the expanded views of the current distributions near the edge at $x = 0$. I_{zt} is the total current flowing along the z direction. Thus the normalised quantity J_z/I_{zt} has units of $1/\text{m}^2$. When we analyse the data at $x = 0.5w$ on Fig. 2 and $x = 0.25w$ on Fig. 3, the current distributions agree with what the skin effect plane analysis⁷ predicts. The current distributions decay as $e^{-\Delta\delta/\delta} \times e^{-j\Delta\delta/\delta}$, where $\Delta\delta$ is the amount of penetration depth into the metal strip. Since J_x has odd sym-

metry, only the right half of the phase information is presented. The left half differs from the right half by 180° .

Surface currents: Fig. 2 shows that J_z at $y = 0$ is approximately a factor of 7.7 larger than at $y = t$. The corresponding factor in Fig. 3 (for J_y) is 1.5. The electromagnetic fields concentrate underneath the conductor strip of Fig. 1 and result in a larger surface current below the conductor strip. Being different from the results obtained by the full-wave analyses assuming infinitely thin perfect conductor, J_x is no longer zero at $x = 0$ (or w) because the conductor strip has finite thickness. When we analyse $|J_z/I_{zt}|$ at $y = 0$ and $y = t$ in Fig. 2, we find that the commonly known singular phenomenon in $\delta^{-1/3}$ variation for a lossless rectangular conductor strip at the corners located at points $(0, 0)$, $(0, t)$, $(w, 0)$, and (w, t) is lost. In fact, according to our analysis, the surface currents increase when the observation point is moving vertically away from the corners at $x = 0$ (or w).

Conclusions: A new full-wave hybrid formulation technique for analysing millimetre-wave planar and/or quasi-planar transmission lines has been developed, and is valid by the theory of skin effect plane analysis when that is applicable. For the case of a microstrip with thick and good metal coating, it is found that the surface current density is no longer singular at the corners of the rectangular metal strip.

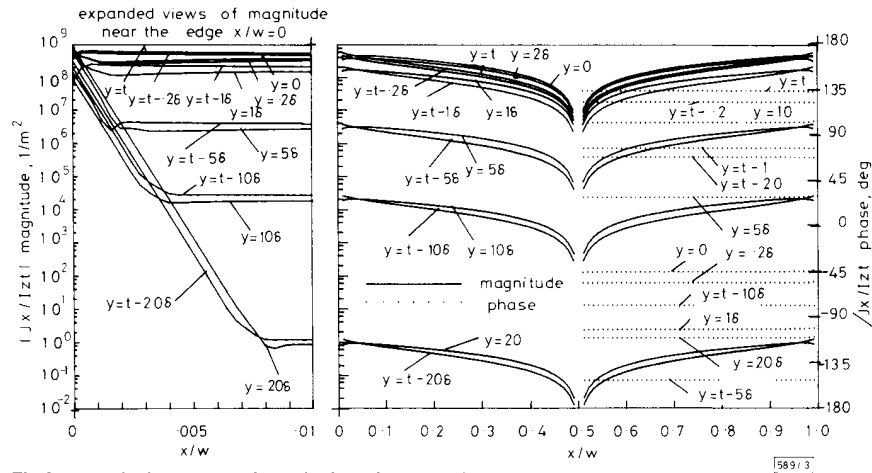


Fig. 2 Longitudinal components of normalised complex current distributions
 I_{zt} = total current in z direction

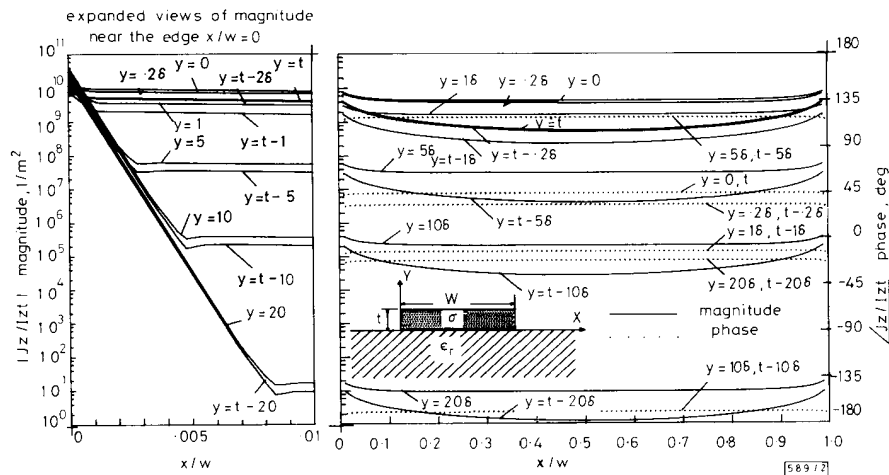


Fig. 3 Transverse components of normalised complex current distributions
 I_{zt} = total current in z direction

This is in contrast to the case of a lossless microstrip line having a rectangular perfect conductor strip which should have $\delta^{-1/3}$ singular field behaviour.

C. K. C. TZUANG
W. K. WANG

18th June 1990

Institute of Communication Engineering
National Chiao Tung University
75, Po-Ai Street
Hsinchu
Taiwan, Republic of China

References

- 1 ITOH, T.: 'Overview of quasi-planar transmission lines', *IEEE Trans.*, 1989, **MTT-37**, pp. 275-280
- 2 JANSEN, R. H., ARNOLD, R. G., and EDDISON, I. G.: 'A comprehensive CAD approach to the design of MMIC's up to mm-wave frequencies', *IEEE Trans.*, 1988, **MTT-36**, pp. 208-219
- 3 HEINRICH, W.: 'The slot line in uniplanar MMIC's: propagation characteristics and loss analysis', 1990, IEEE MTT-S Int. Microwave Symp. Digest, Session D-2, pp. 167-170
- 4 VAN DEVENTER, T. E., KATEHI, P. B., and CANGELLARIS, A. C.: 'An integral equation method for the evaluation of conductor and dielectric losses in high-frequency interconnects', *IEEE Trans.*, 1989, **MTT-37**, pp. 1964-1972
- 5 PENG, S. T., TZUANG, C.-K. C., and CHEN, G.-D.: 'Full-wave analysis of lossy transmission line incorporating the metal modes', 1990, IEEE MTT-S Int. Microwave Symposium Digest, Session D-3, pp. 171-174
- 6 ALTSCHULAR, H. M., and GOLDSTONE, L. O.: 'On network representations of certain obstacles in waveguide regions', *IRE Trans.*, 1959, **MTT-7**, (2), pp. 213-221
- 7 RAMO, S., WHINNERY, J. R., and VAN DUZER, T.: 'Fields and waves in communication electronics' (John Wiley, 1984), 2nd edn., Secs. 3.16 and 4.4

SIMPLE MICROPROCESSOR-BASED LOAD ANGLE MEASUREMENT INSTRUMENT

Indexing terms: Measurement, Microprocessors and micro-processor application

The design and implementation of a simple load angle measurement instrument built around a Z80 microprocessor is described. The task of the microprocessor is to measure the load angle of a synchronous generator which is equal to the phase angle between the internal excitation voltage and the generator output. The load angle is displayed on a on line screen. It is also converted to an analogue value and recorded by an on line plotter for transient analysis a feature that makes such an instrument suitable for either digital or analogue controllers. The tests carried out showed that the instrument has a very fast response. It is accurate, reliable and inexpensive. The resolution in the load angle measurements can be increased by a simple procedure.

Introduction: The load angle of the synchronous machine is conventionally defined as the angle between the phasor of the internal excitation voltage and the phasor terminal voltage of the machine. One of the usual ways to determine the internal excitation voltage is to detect the instantaneous position of the machine rotor.

In power system stability studies load angle measurement is essential because it indicates how close the synchronous machine is to pulling out of synchronism. When it is assumed that the synchronous generator is ideal, with no losses, it will run steadily at no load with the axis of its rotating magnetic field in alignment with its rotor pole axis. As the load applied to the generator increases, the magnetic field starts to fall back from this position, creating a negative load angle.

A transient recording capability of the measuring system is very desirable to control the inputs for the synchronous machine to improve its dynamic behaviour for power system stability enhancement.

Several analogue and digital techniques were used to measure the load angle of the synchronous machine.^{1,3,4} However, most of the methods used require special equipment and the measured angle is still not very accurate. Since microprocessors became available, they have proven to be very attractive in the applications of instrumentation and measurement. They are very flexible in terms of programmability and are simple and inexpensive.

A microprocessor based load angle measurement system has been implemented using a Z80 microprocessor applied to an inverter-driven reluctance motor.² The system response is fast but its implementation is rather complicated.

In this letter a simple microprocessor based instrument for load angle measurement is described.

Implementation of the system: Hardware implementation: The load angle instrument is applied to a synchronous generator driven by a synchronous motor. The system block diagram is shown in Fig. 1. Two signals are produced from the machines.

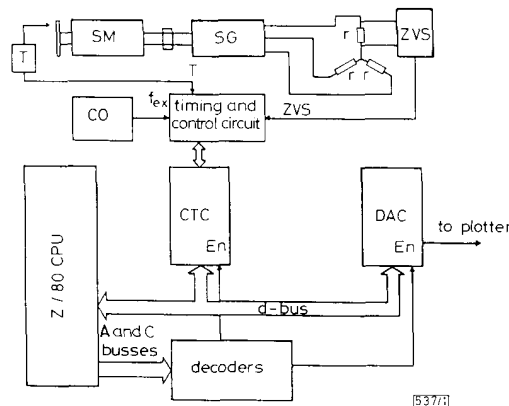


Fig. 1 The load angle measurement instrument system

T: Transducer signal
SM: Synchronous motor
SG: Synchronous generator
ZVS: Zero voltage switch
CO: Crystal oscillator
CTC: Counter/time circuit

The first is the reference rotor angle signal T derived from the rotor angle transducer consisting of a disc with four equidistant black marks mounted on the machine's shaft. A self-contained photo-transistor and light source provide for equally spaced pulses every revolution. The transducer must be positioned in such a way as to give an almost zero angle reading when the generator is on no load. For higher resolution measurements such a condition can not be easily fulfilled. If it is not, it means that the reading of the load angle has some offsets and this can be skipped before the reading being displayed to get the actual reading which equals zero for no load.

The other signal produced from the synchronous machine is the terminal voltage zero-crossing which is generated by a zero voltage switch (ZVS) producing a TTL output pulse whenever the terminal voltage crosses the time axis.

A counter-timer circuit (CTC) interfaced to a Z80 microprocessor counts the number of pulses produced by an external clock for a certain time representing the load angle value.

The CTC is an eight bit programmable counter-timer circuit which is one of the available supporting devices of the Z80 microprocessor system. It has four independent channels, each one can be configured by the microprocessor into different modes by sending the appropriate control and time constant words. Each channel counter has a clock trigger (TR) input which decrements the counter contents by one for every clock trigger pulse.

The counter has a zero count-time out output (ZC) that provides a narrow pulse whenever the counter contents reaches zero. Each channel counter is capable of generating an